

## Thermal history of a pebble in the Indus Molasse at the margin of a Himalayan metamorphic core complex

*M.A. Forster, Lloyd T. White, Talat Ahmad*

Journal of the Virtual Explorer, Electronic Edition, ISSN 1441-8142, volume **38**, paper 4  
In: (Eds.) M.A. Forster and J.D. Fitz Gerald, *The Science of Microstructure - Part II*, 2011.

Download from: <http://virtualexplorer.com.au/article/2011/267/thermal-history-of-a-pebble-in-the-indus-molasse>

Click <http://virtualexplorer.com.au/subscribe/> to subscribe to the Journal of the Virtual Explorer.  
Email [team@virtualexplorer.com.au](mailto:team@virtualexplorer.com.au) to contact a member of the Virtual Explorer team.

Copyright is shared by The Virtual Explorer Pty Ltd with authors of individual contributions. Individual authors may use a single figure and/or a table and/or a brief paragraph or two of text in a subsequent work, provided this work is of a scientific nature, and intended for use in a learned journal, book or other peer reviewed publication. Copies of this article may be made in unlimited numbers for use in a classroom, to further education and science. The Virtual Explorer Pty Ltd is a scientific publisher and intends that appropriate professional standards be met in any of its publications.

# Thermal history of a pebble in the Indus Molasse at the margin of a Himalayan metamorphic core complex

## M.A. Forster

Research School of Earth Sciences, The Australian National University, Canberra, Australia.  
Email: [marnie.forster@anu.edu.au](mailto:marnie.forster@anu.edu.au)

## Lloyd T. White

Research School of Earth Sciences, The Australian National University, Canberra, Australia.

## Talat Ahmad

1. Department of Geology, Delhi University, Delhi, India.
2. Kashmir University, Srinigar, Kashmir, India

**Abstract:** In this paper we report on data from a pebble within an upright fold in the Indus Molasse. The pebble was analysed microstructurally, white mica was separated, irradiated, and subject to  $^{40}\text{Ar}/^{39}\text{Ar}$  geochronology during a step-heating procedure *in vacuo*. Because of the care with which this procedure was followed, the apparent age spectra that resulted was a near perfect replica of what might be expected as the result of diffusional loss of argon from a fractal diffusion network. The earlier reported phenomenon of fractal feathering in the Arrhenius plot is observed in this sample. If the Arrhenius data are analysed so that the Fundamental Asymmetry Principle is obeyed, the inferred diffusion parameters are close to those obtained from high-pressure experiments. These data are then analysed using  $r/r_0$  plots. Two distinct diffusion domain sizes could be recognised, and a pattern of gas release theoretically consistent with fractal feathering of the smaller domain size. The results can be taken to indicate that the pebble was eroded from the Ladakh Batholith some time after 16.5 Ma, during its extensional exhumation, and incorporated in the molasse. The upright folding during inversion of the core complex took place at a later time, i.e. mid-Miocene or younger.

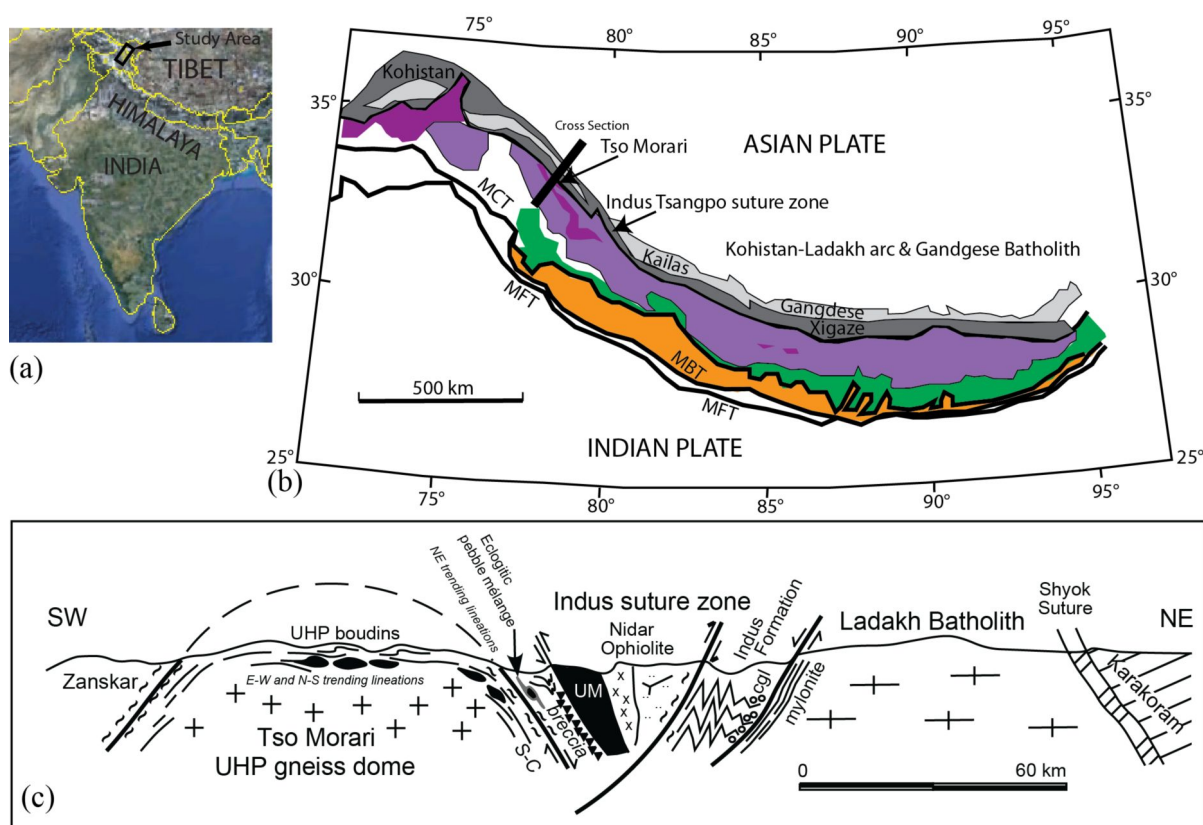
## Introduction

Molasse deposits are important because there is a considerable amount of tectonic detail that can be inferred from their deposition (Davis *et al.* 2004), for example erosion from different uplifted and exhumed parts of an orogeny can be deposited within a single molasse. There are a number of geologically significant molasse zones within the Himalaya mountain belt that have provided information on the evolution in both time and space of this mountain belt (e.g., Aitchison *et al.* 2002; Davis *et al.* 2004; Garzanti and Van Haver 1988; Rowley 1996; Sinclair *et al.* 2001): In the Siwalik Basin located in the Nepalese section of the Himalaya, there is a widespread

molasse sequence along the foothills of the Himalaya (Najman *et al.* 2004); The Gangrinboche conglomerates bound the length of the Yarlung Tsangpo suture zone on the southern margin of the Lhasa terrane in the north of the Himalaya region (Aitchison *et al.* 2011); In south-central Tibet there is the Kailas conglomerate; The Bakiya Khola molasse in southeastern Nepal (Davis *et al.* 2004; Gansser 1980); and the Indus molasse lies fragmented along the Indus suture zone in NW of India.

It is the Indus molasse on which this study is based (Fig. 1). These molasse are all laterally extensive but occur at different locations on the Himalaya belt.

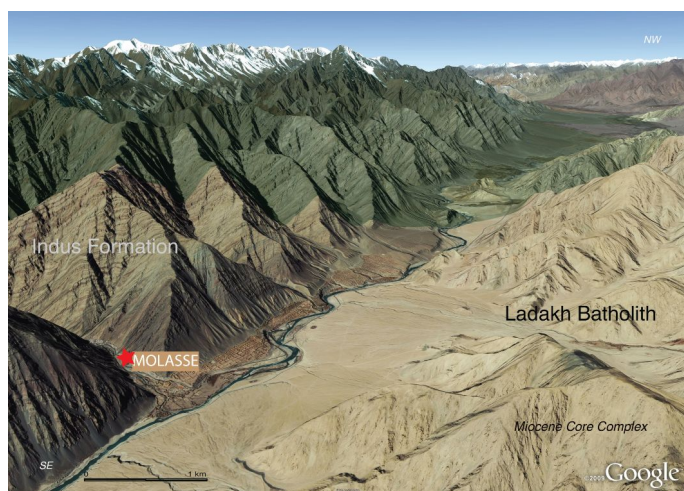
Figure 1. Location of the study area.



(a) Map of NW India with the study area marked as rectangle (From: Google Earth); (b) Plan view of geological map of the Himalaya defining the major geological units. Our sample of the Indus Molasse comes from the Indus Tsangpo suture zone, which is dark grey in colour. Note: Kohistan-Ladakh arc and Gangdese batholith is light grey colour; Tso Morari/Tethyan metamorphic rocks in purple colour; orange is the lesser Himalayan Sequence; and dark green the Higher Himalayan Crystallines (modified from Guillot *et al.* 2008); (c) Schematic cross-section defining the major geological features in the NW Himalaya that include major structures such as the Zanskar, Tso Morari dome, Indus Formation and Ladakh Batholith. Note that location of the cross section is marked in (b) with heavy black line. The area of interest to this study is the northern section of the Indus Formation with a conglomerate zone immediately adjacent to the Ladakh Batholith (scale bar is given simply as a guide and overall distances are not to scale).

They are all laterally extensive along the length of the belt and in their location within the orogeny (perpendicular to the belt) from adjacent to the Main Front Thrust to the zones well behind the Indus Suture. The source of material in the molasse (e.g. pebbles) would thus be specific to the tectonic processes operating at that point in the orogeny at the time of their formation. The Indus Molasse is important due to its location adjacent to the Indus Suture and the tectonics relating to collision of India and Asia.

Figure 2. Google image of the Indus suture region.



The location of the pebble is marked by the red star on the boundary of the Indus Formation. The Indus River located diagonally along the centre of the map marks the boundary of the Indus Formation and the structurally underlying Ladakh Batholith on the right hand side of the image. The map is sourced from Google Earth: The pebble sample collection site (marked with a red star) is at 3,256 metres altitude at N: 33° 48' 79.4"; E: 77° 48' 63.8" ±14 metres.

Studies as early as the 1900s (e.g. by the Geological Survey of India) on the different molasse in the Himalaya shows an early recognition of their importance. These early studies provided observational information on the age and provenance of granitic pebbles in conglomerate zones (Auden 1933). The Himalayan molasse zones have provided a wealth of geological information, on tectonics (e.g., Searle *et al.* 1990, Harrison *et al.* 1993, Clift *et al.* 2002, Schlup *et al.* 2003), for geochemical and geochronological studies of provenance, erosion and drainage (e.g., Harrison *et al.* 1993, Clift *et al.* 2001), depositional rates, uplift characteristics, unroofing and cooling rates (Harrison *et al.* 1993), and the evolution of regional climate change (e.g., Harrison *et al.* 1993, Stern *et al.*

1997). Laterally extensive molasse units in the northern Himalaya region are a direct response to the orogen-scale tectonic processes caused by the India-Asia collision, recording aspects of its development (Aitchison *et al.* 2002). Similarly, the more southern extensive but fragmented Indus molasse also reflects regional-scale tectonics, extension and shortening events during the evolution of the mountain belt.

Thermochronological studies using  $^{40}\text{Ar}/^{39}\text{Ar}$  geochronology can be used to calculate tectonic rates (e.g., unroofing, uplift, cooling) and chronostratigraphy that would otherwise be difficult to determine. This has been done at several locations on molasse in the Himalaya, for example in southeastern Nepal on the Bakiya Khola, where the molasse is laterally extensive and lies between the Main Boundary Thrust and the Main Frontal Thrust. In this case  $^{40}\text{Ar}/^{39}\text{Ar}$  geochronology was undertaken to ascertain depositional ages that were then used to interpret the regional exhumation history (Harrison *et al.* 1993). In south-central Tibet Harrison *et al.* (1993, their figures 1, 2) have studied the Kailas conglomerate and provided  $^{40}\text{Ar}/^{39}\text{Ar}$  cooling ages from which they have studied the rates and duration of uplift.

The Indus Molasse (equals the Kardong Formation in Thakur and Misra 1984) generally lies on the southern banks of the Indus River, in the NW Himalaya in Ladakh (Figure 1) and initially overlay the Indus Formation (prior to later folding and inversion, Figure 2). The northern boundary of the Indus Formation is irregularly bounded by this molasse that has accumulated as the result of erosion of the adjacent batholith and hence also includes pebbles from the batholith and leucogranite dyke swarms. The pebbles in the molasse at the study location also include ophiolitic material and perhaps pebbles from further afield (Figure 3a). We cannot be precise as to the exact location of their sources (cf Wu *et al.* 2007). What we can say is that the pebbles have been transported from an exhumed or exhuming and eroding igneous body and subsequently buried after their initial deposition, consolidated then folded during back thrusting over the Ladakh Batholith.

The southern margin of the Ladakh Batholith is occasionally bounded by S/SW-dipping ductile shear zones (e.g., N 33° 53' 31.6", E: 77° 45' 34.2"). These structures may well define remnants of the carapace shear zone of a metamorphic core complex, although few data are currently available to support this hypothesis.

Figure 3. The Indus Formation with the suspected source of the pebble.



(a) Molasse with a variety of pebbles from different protoliths (image 700 mm wide); (b) Sedimentary layering in the Indus Formation with overprinting slaty cleavage in the shale and pull-aparts in the competent layer (image ~10 cm wide); (c) A representative pebble sourced from the Ladakh Batholith used in this study (pebble ~14 cm wide, ~21 cm long); (d) Ladakh Batholith with abundant leucogranites, located at the southern boundary of the batholith, the photograph has been taken near Chumathang, at the boundary of the Indus Suture zone (image ~800 m wide in foreground).

These shear zones appear to be extensional in character, with a regional south-directed normal-sense of movement. If this hypothesis is correct, parts of the Indus Formation are a molasse that formed as an apron at the margins of the Ladakh core complex, after its exhumation, once the lower plate was exposed. Later inversion resulted in back thrusting of the molasse over the Ladakh Batholith, during which episodes of recumbent then tight upright folds formed in the molasse. Pervasive axial plane fabrics developed during this later folding, overprinting the earlier formed structures. Here we report argon geochronology that allows constraint on the age of deposition of a pebble (Figure 3c) collected from a bed of the Indus molasse. The molasse at this location has subsequently been folded, and backthrust over the Ladakh Batholith.

### Pebbles within the Indus Molasse

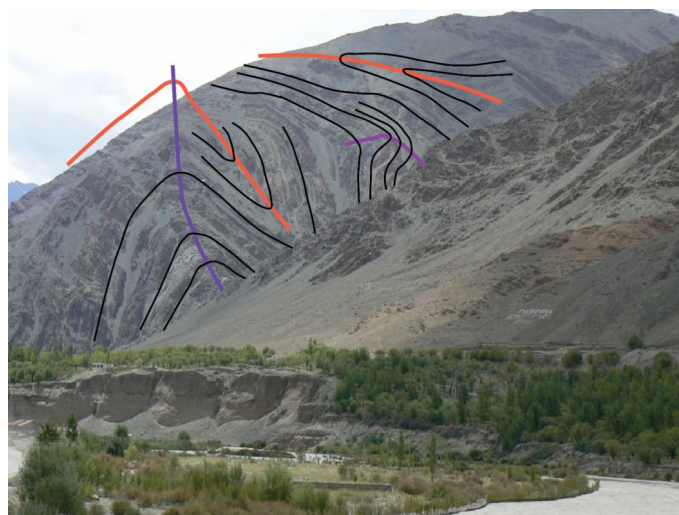
The molasse displays an overall decrease in pebble size away from the northern tectonic contact (i.e. larger pebbles occur at the contact compared to the distal zone). The percentage of pebbles in the groundmass of the molasse also decreases away from the northern contact, suggesting the initial deposition was adjacent to the batholith. The pebbles from our study location vary in size and character (e.g., rock type and protolith), ranging in size from ~3 cm to ~30 cm. Water tumbling and abrasion during transportation has produced rounded pebbles. The pebbles themselves have well-preserved original mineralogy and microfabrics (Figure 3). Weathering has not taken place and the pebbles are exceptionally well preserved. Note that the term pebble used in this paper refers to the layman use of the term and that the official terminology should be cobble but is not used here (*cf.* pebble (4mm-16mm), cobble (16mm-256mm) and boulder (>256mm)).

The most prominent geomorphical features in the Indus Formation are bedding and a pervasive and penetrative slaty cleavage overprint. This cleavage occurs only within the shaley non-competent layers (Figure 3b) and is axial planar to large-scale upright folds (Figure 4). The overlying Indus Molasse is also affected by this folding event. In addition a previous recumbent folding event is preserved within the limbs of the upright folds (Figure 4).

As mentioned above the molasse is folded by the same generation upright folding as the underlying Indus

Formation, however in the molasse the folding is on a smaller-scale. The pervasive axial planar fabric also occurs in the molasse, however it is not well-defined. For example, the fabric in the molasse is discernible but weak and anastomoses around even the small pebbles and commonly lies along the weaker zones (Figure 5).

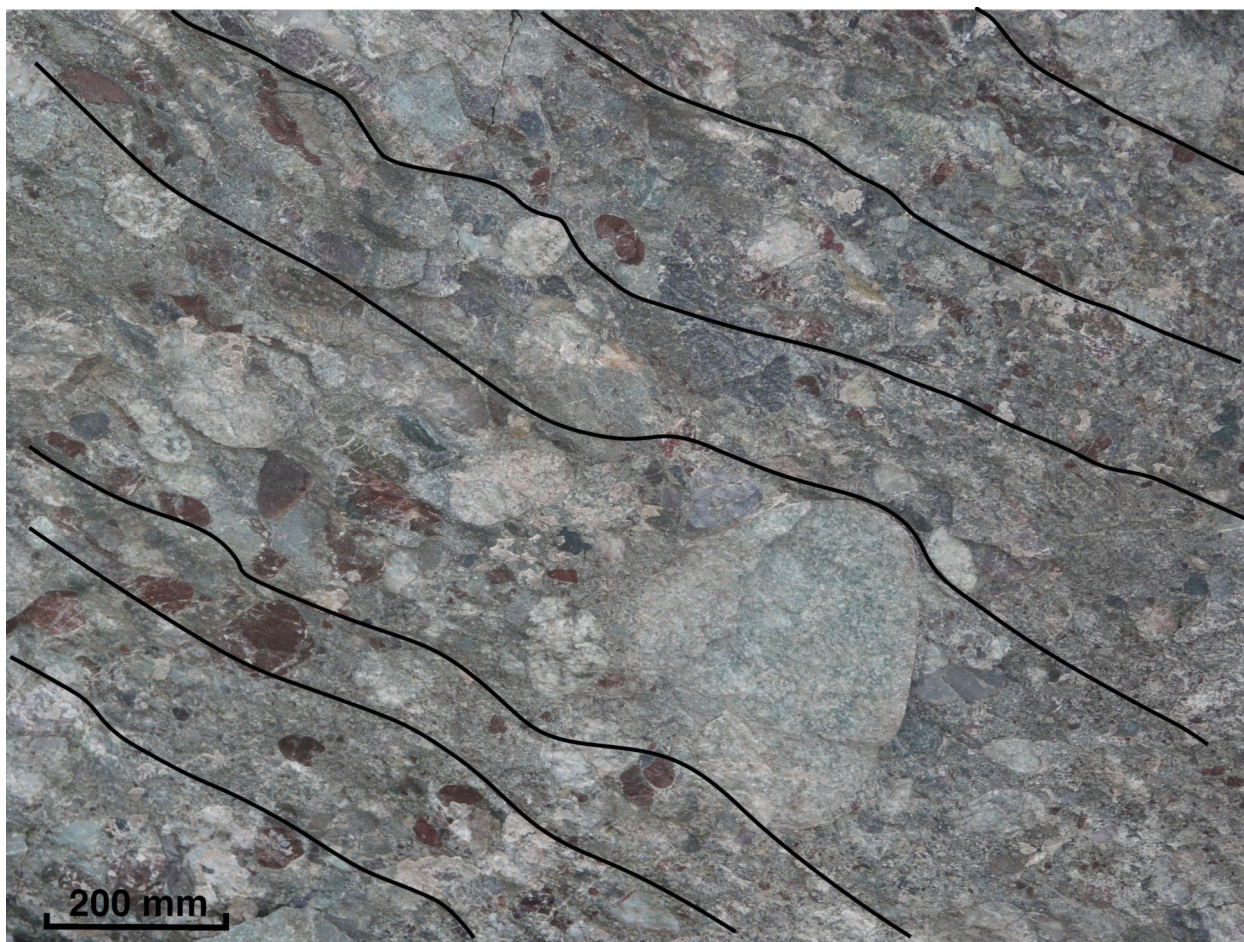
Figure 4. Folded Indus Formation.



When the Indus Formation is viewed approximately perpendicular to the contact with the Ladakh Batholith (along strike of the Indus suture), several generations of folding are observed. The older generation of folds are characterised as recumbent folds (the axial plane marked in red = FR), these are overprinted by a younger upright folding event (FU) with the axial plane marked in purple (therefore the FR is followed by FU). The multiply-folded fabric is highlighted with black lines. The upright folds are on the scale of hundreds of metres. The upright fold nearest the river is approximately 300 metres in the gully.

The deformational fabrics in the structurally lower zones of the molasse were observed to be more intense closer to the contact with the Ladakh Batholith. In contrast, the Indus Formation displays spectacular original depositional layering that can be observed from the air as one flies into Leh, or with satellite imagery such as displayed on Google Earth. The deposition of the Indus Formation was independent to the overlying molasse, however after the period of deposition of the molasse (Thakur and Misra 1984), both units were then deformed as a single unit.

Figure 5. Example of the molasse.



The molasse has been folded with the underlying Indus Formation. The deformational fabric that has formed within the molasse due to the folding, is irregular in character and anastomoses around the larger pebbles (rocks) and irregularities in the molasse. Even though the fabric is irregular, it occurs on the mm-scale. It is not brittle jointing.

The structures with the Indus Molasse and the Indus Formation do not resemble those within the Ladakh Batholith (e.g. the Thanglasgo Shear Zone of Weinberg and Dunlap 2000).

### Tectonic understanding from the micro-scale analysis of the pebble

The essence of this paper is to show how a single pebble, in fact a few grains from a pebble from the molasse can influence our understanding of a tectonically significant event as great as the India/Asia collision. The key to this study is to show that microstructural analysis and microchemical data can provide key information to the regional and even plate-scale tectonics.

The selection of the pebble from such an extensive molasse was done with the following criteria: 1) to choose a representative sample that is common within the

molasse; 2) that it is a well preserved so that analyse can be undertaken in order to produce quality data; and 3) that minerals within the sample are of the right composition to allow geochronology on the preserved deformational or metamorphic events that still remain in this small exotic rock. Such a pebble was selected. It is a rounded pristine granitic pebble containing aligned white mica grains thus preserving both deformational information and possible igneous and/or metamorphic information. Minerals in the sample are suitable to be dated using  $^{40}\text{Ar}/^{39}\text{Ar}$  geochronology to determine both timing and duration of events.

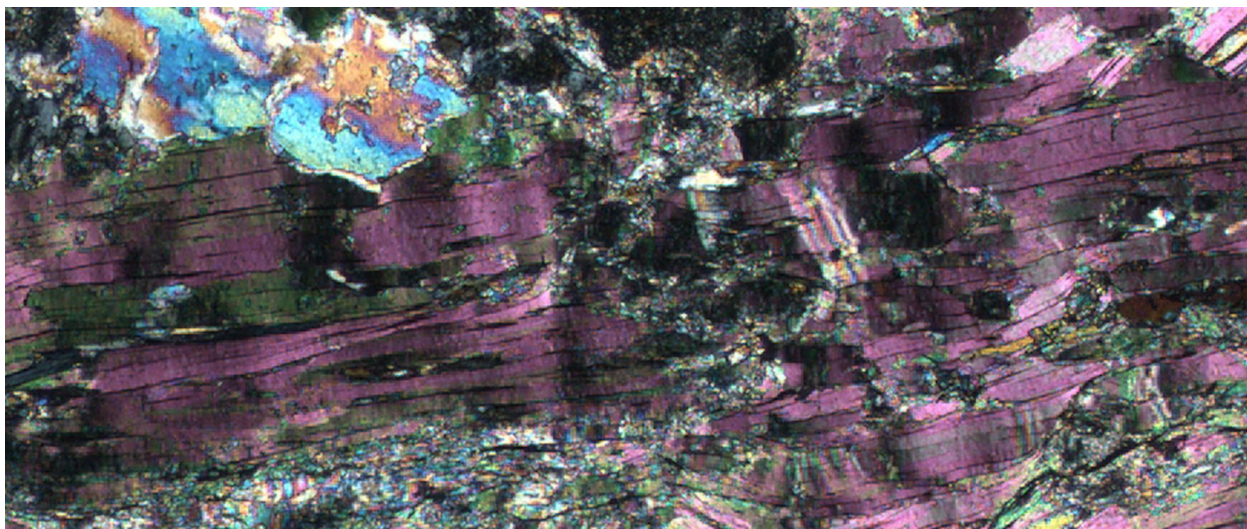
### Microstructural and microchemical analysis

It is vital that all micro-scale information be directly linked to the local and the regional structural geological framework. Microstructural analysis of the pebble was

done to quantify the character of the pebble itself, and to determine deformation patterns and the quality of individual grains. Microchemical analysis was undertaken to provide information on the variation between possible

different generations of white mica grains, and any intra-grain changes and character of the white micas. This combined data has been essential for the understanding of the  $^{40}\text{Ar}/^{39}\text{Ar}$  geochronology undertaken in this study.

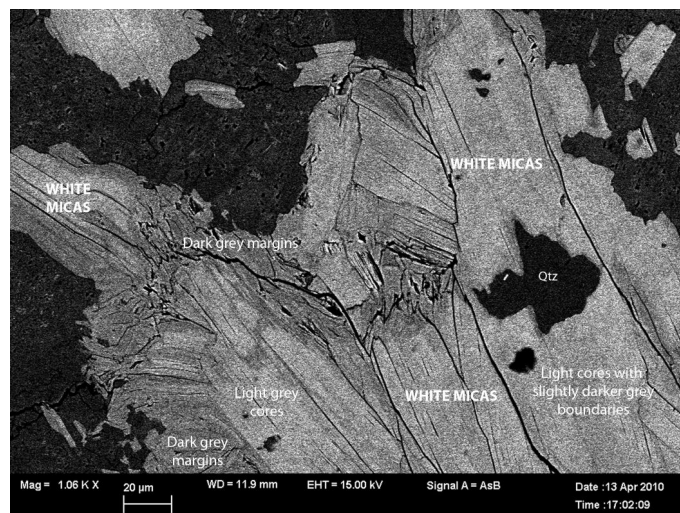
Figure 6. Microphotograph of white mica zones.



White micas with grain-scale deformation. Recrystallisation occurred mainly at the margins and adjacent to defects. Irregular deformed high-strain zones remain frozen into the grains. Field of view ~5 mm.

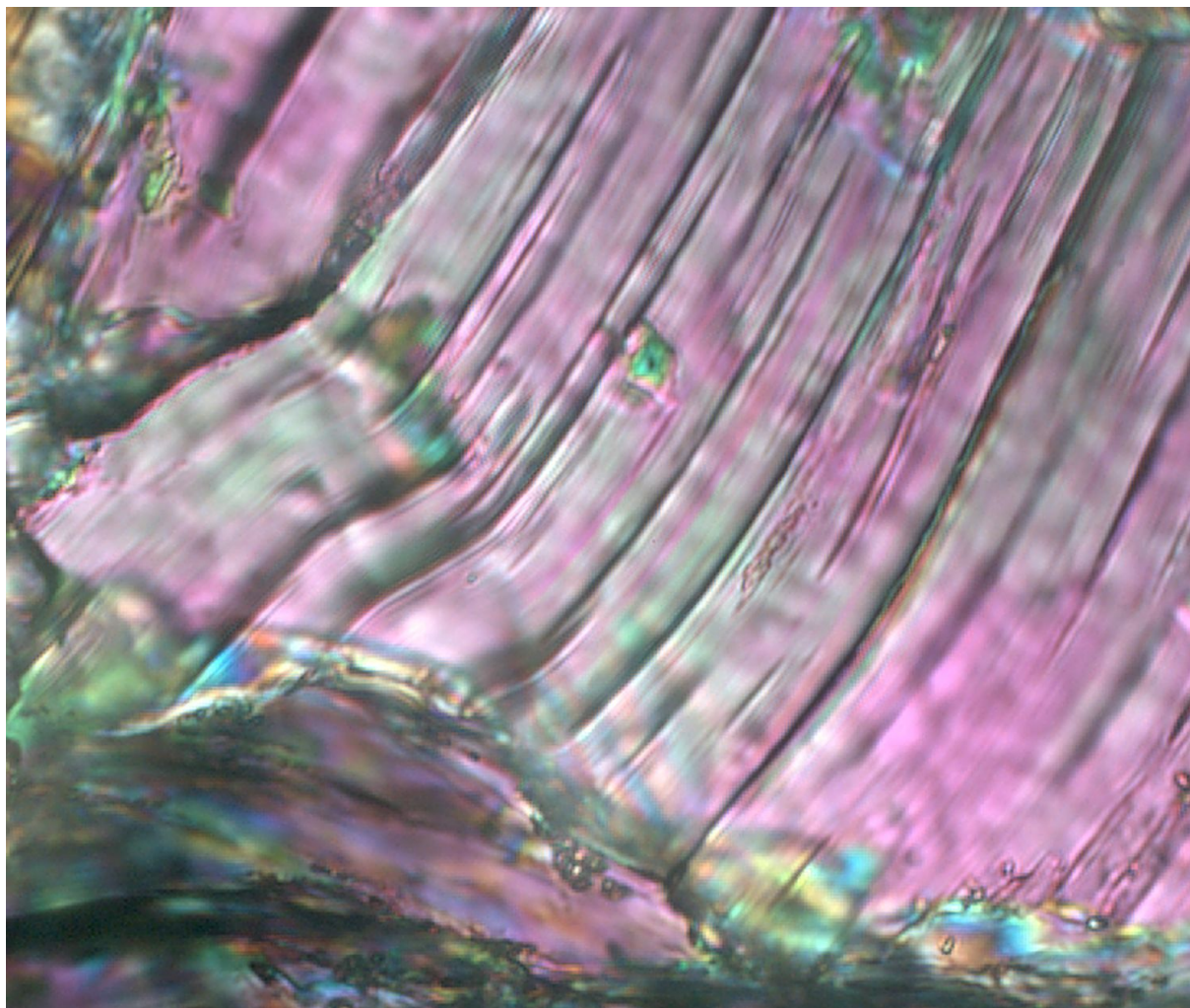
The granite pebble used in this study contains isolated zones of aligned white micas that anastomose across the whole pebble. White mica grains do occur elsewhere in the pebble but are rare (Figure 3b). Microstructurally the narrow zones of white mica grains represent a deformational fabric or micro-scale shear zone (Figure 6). These white mica-rich zones are commonly 2-4 grains thick with grains up to 1:10 W:L ratio, however not all grains remain as whole grains due to fracturing and significant internal deformation. For example, some grains are themselves folded, generally with the fold axis perpendicular to the long edge of the grain. Also irregular kinks of single grains occur causing extensive irregular undulose extinction (Figures 6, 7, 8). In addition complete and partial fracturing of the grains is common phenomena (Figure 9). Micro-scale localised recrystallisation is observed around the margins of grains and in zones at the boundaries of fractures, or high strain zones (Figures 7, 8 and 9). A greater degree of recrystallisation is present in the smaller grains compared to the larger elongate grains.

Figure 7. Backscatter image of several grains of white mica indicating the variation in composition using tonal variation (dark to light grey).



Note the scale in bar below image.

Figure 8. Microphotograph of deformed white mica with little to no recrystallisation occurring along high strain zone.



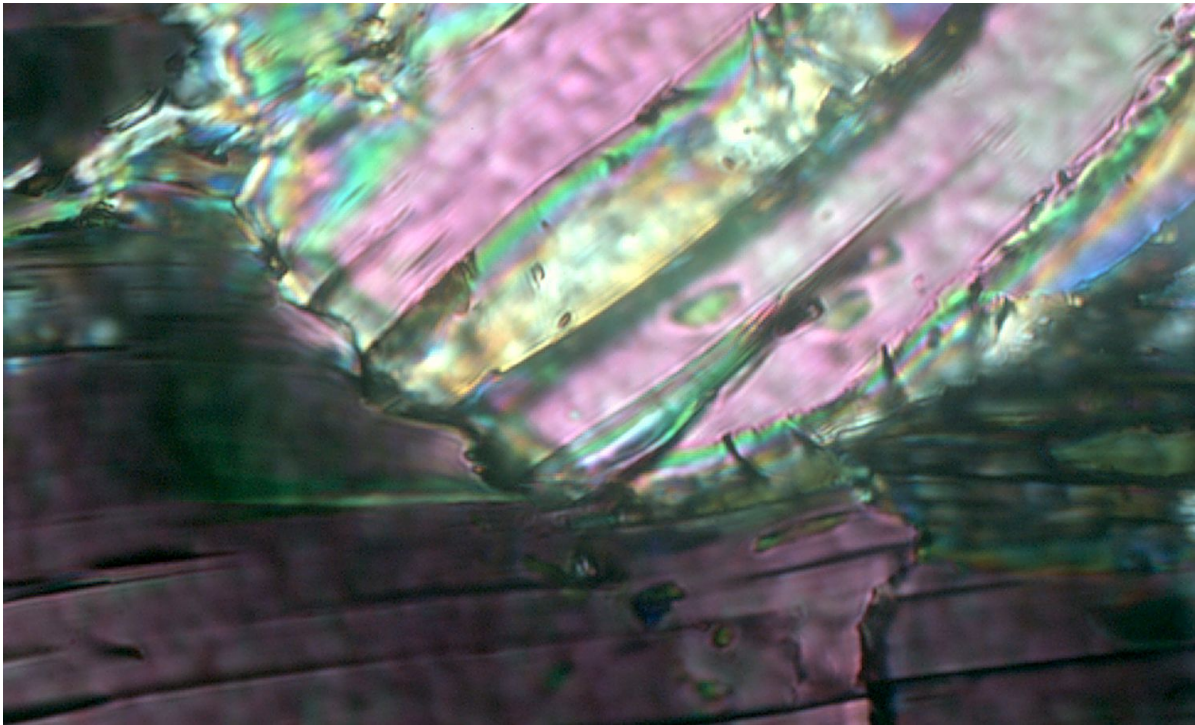
Scale: Field of view ~60  $\mu\text{m}$ .

Backscatter images verified intra-grain deformation and localised crystallisation of the white micas. Images of the white mica grains within these small-scale shear zones showed a chemical variation, recorded as three different tones within and between white micas (Figure 7). Micro-chemical analysis of the different shaded zones was undertaken to determine any differences in composition, three different compositions of white micas were detected, the lighter core was the dominant composition. A mid-grey rim to the core was common as it rimmed all the light grey zones, however it was a narrow zonation. The third chemical composition was the darker regions. The recrystallisation seen as the darker areas in the backscatter image, is not as abundant as the core composition and occurred on the very margin, fractured terminations to grains were generally completely recrystallised, as

were simple fractured zones. Any new white mica grew as small grains and also had this chemical composition.

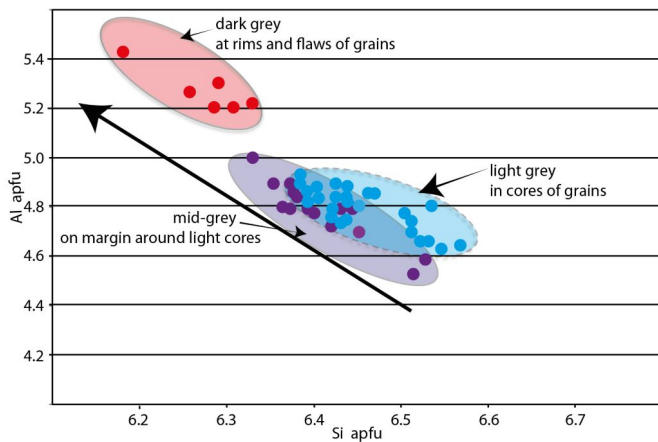
When these three different microchemical compositions are plotted on an Al/Si apfu (Atomic Per Formula Unit) plot (Figure 10) it can be observed that the texturally younger, dark zones (observed in the back scatter image) are microchemically distinct (low Si apfu) when compared with the cores. The older cores of the grains (light grey) and the rims of the cores (middle-grey) overlap on the plot with the lighter cores having the highest Si-content numbers. The micro-chemical results of the three different generations of white mica show a distinct shift from higher Si-content of almost 6.6 (Si apfu) in the white mica cores to a low of just under 6.2 (Si apfu) in the darker rims of small grains, reflecting a decrease in pressure with later crystallization (Bröcker *et al.* 1993 ).

Figure 9. Microphotograph of recrystallisation at the terminal point of a broken white mica.



Scale: Field of view ~70 µm.

Figure 10. Graph of microchemical variation defined by Si- and Al-apfu (Atomic Per Formula Unit).



The cores of grains had slightly higher Si-apfu, however mostly there is very minor variation compared to the rims of these grains. A generation of white mica growth, defined as a darker grey in the backscatter image, Figure 7, has distinctly lower Si-apfu compared to cores. These growth areas are minor in the overall volume of the analysis of white micas from this pebble.

## Geochronology

The geochronometer used in this study is  $^{40}\text{Ar}/^{39}\text{Ar}$  geochronology, however SHRIMP U/Pb geochronology has been done in the adjacent Ladakh Batholith (White *et al.* 2011 cf Wu *et al.* 2007) and is referred to here to correlate ages of the igneous bodies in the region so as to verify the possible source of the pebble analysed using  $^{40}\text{Ar}/^{39}\text{Ar}$  geochronology.  $^{40}\text{Ar}/^{39}\text{Ar}$  geochronology has been used to analyse this pebble due to the versatility of the chronometer. Ages may be obtained from preserved original igneous grains or relict populations, as well as metamorphic grains from younger heating events where cooling ages may be preserved. In addition, information from grains that have been deformed and/or recrystallised in younger events may also be preserved. Relict igneous events can then be correlated with U/Pb SHRIMP ages, metamorphic and recrystallisation can be correlated to the microstructural and micro-chemical results.

### $^{40}\text{Ar}/^{39}\text{Ar}$ geochronological analysis

White micas occur as 'books' of grains aligned in micro-scale shear zones (Figure 6) within a groundmass that is mica-poor. White micas within the groundmass are very small (<20 µm), are interstitial to other larger grains

and have not been analysed due to their fine-grained nature. In contrast, the white micas in the mica-rich zones are characteristically large (<1000  $\mu\text{m}$ ) but also some small grains occur (~100  $\mu\text{m}$ ). It is the grains from these zones that have been used in this argon geochronology study. Grains selected for analysis included grains that were between 150  $\mu\text{m}$  and 350  $\mu\text{m}$ . Smaller grains, seen as the darker grains in the backscatter image, were not selected so as to eliminate potential recoil during analysis. However these darker regions still occur in the analysis at the margins and ends of larger grains.

A carefully designed furnace step-heating experiment on the irradiated white mica was carried out. Particular care was taken monitoring background levels and maintaining low levels of contamination both at the start and during analysis. The furnace itself was checked for contamination and degassed four times to 1450  $^{\circ}\text{C}$  for 30 minutes. A total of 33 mg of single grains are wrapped in tin foil and dropped into the furnace where the foil was melted and then left at 420  $^{\circ}\text{C}$  overnight for contaminants (e.g.,  $\text{H}_2\text{O}$ ,  $\text{CO}_2$ ) to be pumped away prior to analysis. The first step began at 450  $^{\circ}\text{C}$ , 26 steps were run in total with the heating schedule set so as to maintain the percentage of gas release as even as possible over the experiment.

The apparent age spectrum (Figure 11) that resulted from the step-heating experiment is as near perfect replica of what might be expected as the result of diffusional loss of argon from a fractal diffusion network (McDougall and Harrison 1999). The repetitiveness of degassing the furnace and extra time taken with these 'cleaning' procedures has decreased the contamination in the results. Likewise the extensive heating schedule starting at 450  $^{\circ}\text{C}$  has reduced the mixing of different gas populations and allowed the degassing of different gas populations to be released independently and be recorded.

The apparent age spectrum has five steps (between 910-990  $^{\circ}\text{C}$  of the schedule) that record an age of 55.7  $\pm 0.3$  Ma (MSWD 11.9) (with an overall  $^{39}\text{Ar}$  release of 38.5%). An older age of 61.1  $\pm 0.3$  Ma occurs towards the end of the experiment (Table 1 in Appendix A.). The York Plot (Figure 11c) shows a cluster of points, that correspond to the 55.7 Ma steps on the age spectrum, and mixing points up to the 61.1 Ma step. This implies that a range between 55.7 Ma and 61.1 Ma is possible.

The initial steps released very low  $^{39}\text{Ar}$  and give the youngest gas populations. The first step (with 0.05%  $^{39}\text{Ar}$

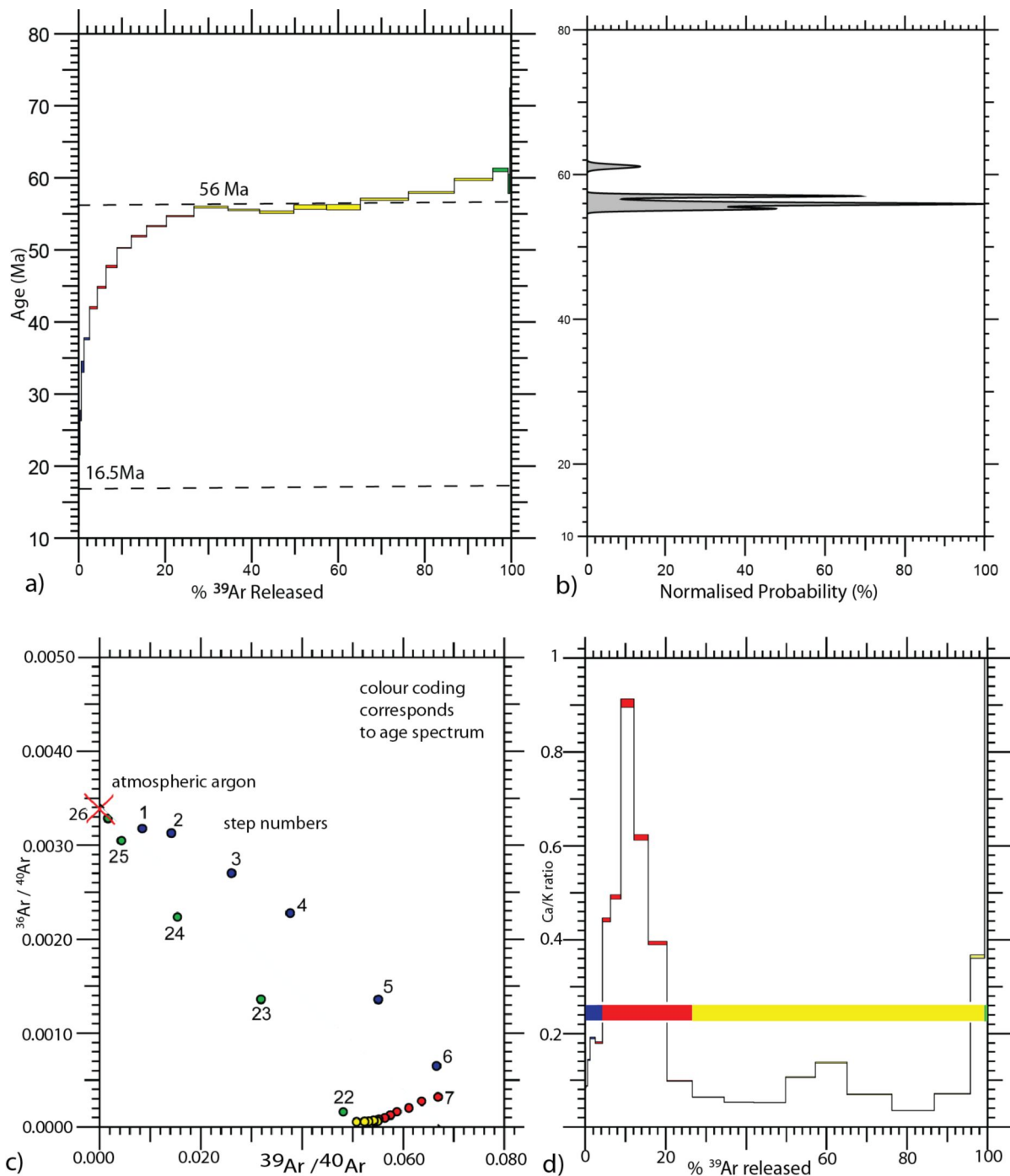
release) is at 22.7  $\pm 10.3$  Ma (a high error), however the second step gives an age of 16.5  $\pm 4.7$  Ma from with 0.10%  $^{39}\text{Ar}$  release. The steps from 1 to 6 have variable amounts of atmospheric Ar, followed by a moderate diffusion loss from step 7 (740  $^{\circ}\text{C}$ ) to the plateau at 55.7  $\pm 0.3$  Ma.

The age spectrum from the white mica shows characteristics of diffusive Ar loss, with a  $^{39}\text{Ar}$  release pattern comparable to K-feldspar diffusion experiments and associated fractal feathering where information on different domains is preserved (Forster and Lister 2010). As a consequence simulation and modelling has been possible on white mica, a process normally restricted to K-feldspars (Lovera *et al.* 1997), which has allowed us to test if the results had geological meaning.

The Arrhenius plots presented in  $^{40}\text{Ar}/^{39}\text{Ar}$  geochronology reflect the pattern of gas release from the different microstructural reservoirs or diffusion domains within the analysed grains. These data can be analysed to extract the activation energy and frequency factor normalised against the square of the diffusion domain radius. Theory for this purpose is set out for modelling K-feldspars using multiple diffusion-domain theory (or MDD models, Lovera *et al.* 1997). When Arrhenius data are analysed assuming a MDD model, the Fundamental Asymmetry Principle (FAP) must be obeyed (Forster and Lister 2010). The Fundamental Asymmetry Principle (or FAP) is implicit in any MDD model. "The FAP applies to any line fitted to data from a sequence of step-heating experiments in which the temperature applied from step to step may be the same, or higher, but may not decrease. Lovera *et al.* (1997) set out the basis of the MDD method, and shows how a straight line can be fitted to a set of Arrhenius data points, under specific circumstances. The fitted line will faithfully replicate the essential Arrhenius parameters only as long as the data points are derived from a set of partially degassed diffusion domains. Mathematically, to be consistent with a MDD model, any line fitted to any sequence of Arrhenius points must divide the population by rank order. Points from data obtained earlier in the sequence of step-heating experiments must lie on the fitted line, or to the right of it. Points from data obtained later in the sequence must lie on the fitted line, or to the left of it. A feathering effect is observed when the smaller diffusion domains are very much smaller than the larger domains" (Forster and Lister 2010, page 23). If the FAP is violated a derived MDD model will produce erroneous

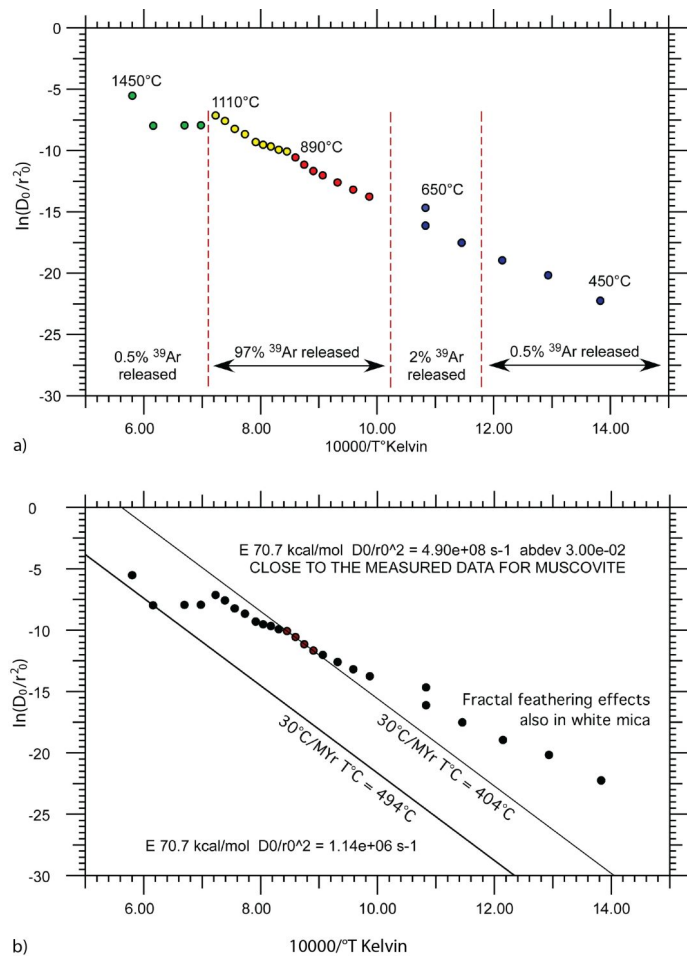
results, for numerically the method utilised will lead to consistently underestimated values for the activation energy ( $E$ ) and for the normalised frequency factor ( $D0/r^2$ ).

Figure 11.  $^{40}\text{Ar}/^{39}\text{Ar}$  apparent age spectrum



a)  $^{40}\text{Ar}/^{39}\text{Ar}$  apparent age spectrum, the first step and plateau at the mid-temperatures of the experiment are marked with a dashed line. The green and final four steps represent the break down of the grains. Spectrum is colour coded so as to be able to correlate with the other graphs; b) Gaussian plot highlighting main gas release %; c) York plot with the points labelled with their step number and colour coded to match other graphs; d) Ca/K plot also colour coded to match other graphs.

Figure 12. Arrhenius plot for white mica experiment

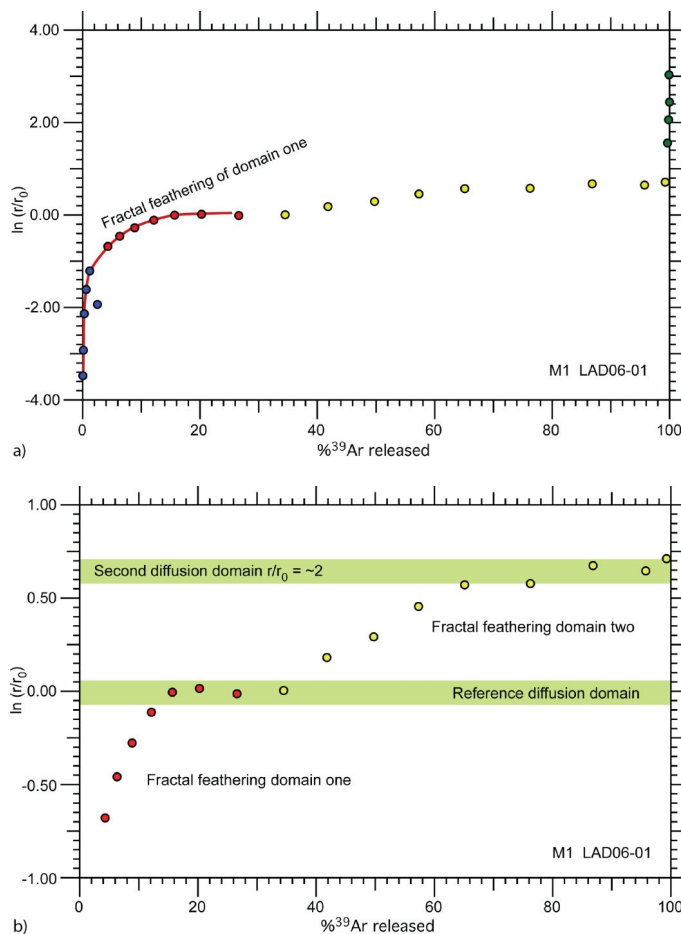


a) % gas release illustrated for the different stages of the apparent age spectra. The cusp point between the yellow and red mark the point of fractal feathering observed in b); b) Arrhenius plot obeying the Fundamental Asymmetry Principle, important in this experiment as the fractal feathering affects are prominent feature of this white mica. The activation energy is calculated using this principle.

One of the important points in this study however is to illustrate that the Arrhenius plots derived from step-heating experiments using white mica can be analysed in a way that is consistent with the FAP (Figure 12). The inferred diffusion parameters produce a retentivity that is not greatly dissimilar to that obtained from high-pressure experiments (Harrison *et al.* 2009). The activation energy from this study was higher (70.7 kcal/mol) but this is in part compensated for by the values for the normalised frequency factor ( $D_0/r^2$ ). Having accomplished this step, it is then possible to derive an  $r/r_0$  plot following methods set out by Lovera *et al.* (1997). Two distinct domain sizes

can be recognised with fractal feathering of related size-volume distributions occurring for both domains (Figure 13). The two domains are different in size by about a factor of two and the pattern of gas release theoretically consistent with fractal feathering of the smaller domain size can be readily observed in the apparent age spectrum (Figure 13).

Figure 13.  $r/r_0$  plot



a) An  $r/r_0$  plot where points form a relatively flat line (see green bands) it marks distinct domain sizes; a rise to an asymptote in the blue then the red steps represent a domain, repeated with the yellow points; an almost perfect example of what should be expected for fractal feathering; b) same as previous slide except larger scale, the blue green steps omitted. At this scale it is more distinct that two distinct domain sizes in the  $r/r_0$  plot occur. Importantly one domain, with the older ages, is twice as thick as the other; both have fractal feathering.

### SHRIMP geochronological analysis

The Ladakh Batholith in the region that could have sourced the granite pebble was sampled. Locations were

at Khardung La granite (LAD06-23: N 34° 16' 41.64"; E 77° 36' 19.49") and the Chang La granite (LAD06-27: N 34° 04' 06.12"; E 77° 56' 33.12") and are approximately 50km apart.

These two granite samples were analysed using SHRIMP U/Pb geochronology with ages being from the cores of zircons: the Khardung La granite giving an age of  $56.8 \pm 0.5$  Ma and Chang La granite giving an age of  $58.0 \pm 0.5$  Ma (White *et al.* 2011). The Khardung La granite correlates well with the  $^{40}\text{Ar}/^{39}\text{Ar}$  plateau age of  $55.7 \pm 0.3$  Ma, while the Chang La age correlates with the  $^{40}\text{Ar}/^{39}\text{Ar}$  age range where the interpretation of a range between  $55.7 \pm 0.3$  Ma and  $61.1 \pm 0.3$  Ma is suggested.

## Discussion

Microstructural analysis of a single pebble from the Indus Formation, within the context of a meso-scale structural framework, has provided useful information for regional and tectonic-scale analysis at this significant location at the Asia/India plate boundary. The inclusion of microstructurally focussed  $^{40}\text{Ar}/^{39}\text{Ar}$  geochronology on characterised grains within the pebble provides the time component to this history which includes information on both absolute time as well as relative timing of events on the broader scale. The Arrhenius data from this  $^{40}\text{Ar}/^{39}\text{Ar}$  step-heating experiment undertaken in this study is of such quality that multiple-diffusion domain experiments and modeling normally only done on K-feldspars has been successfully undertaken on white mica. Thus these diffusion experiments have provided information on the relative sizes of different domains and ages preserved on those domains.

More than one gas reservoir (domains of different ages) is preserved in the white mica from the pebble. The smallest domain represents the least retentive sites and is very small. Nevertheless, this domain constrains the timing of cooling below  $\sim 200^\circ\text{C}$  at  $16.5 \pm 4.7$  Ma. This small domain may have formed during deformation and recrystallization that occurred after the initial cooling of the batholith. In contrast the initial cooling of the batholith is recorded by the main domain with a plateau age of  $55.7 \pm 0.3$  Ma (>30% of gas release) and is the most prominent feature in the apparent age spectrum. This plateau age may reflect a cooling age which is comparable to the SHRIMP ages obtained from the Chumathang leucogranite dyke swarm. In addition, the final stages of the apparent age spectrum show an increase in age up to 61.1

$\pm 0.3$  Ma, which is consistent with a minimum age estimate for cooling of the Ladakh Batholith. Because the argon system within the pebbles has not been reheated to temperatures or conditions that would have reset the system, the pebble has preserved these distinct gas reservoirs and allowed modelling on the cooling history or any recrystallisation that may have occurred during this tectonic process.

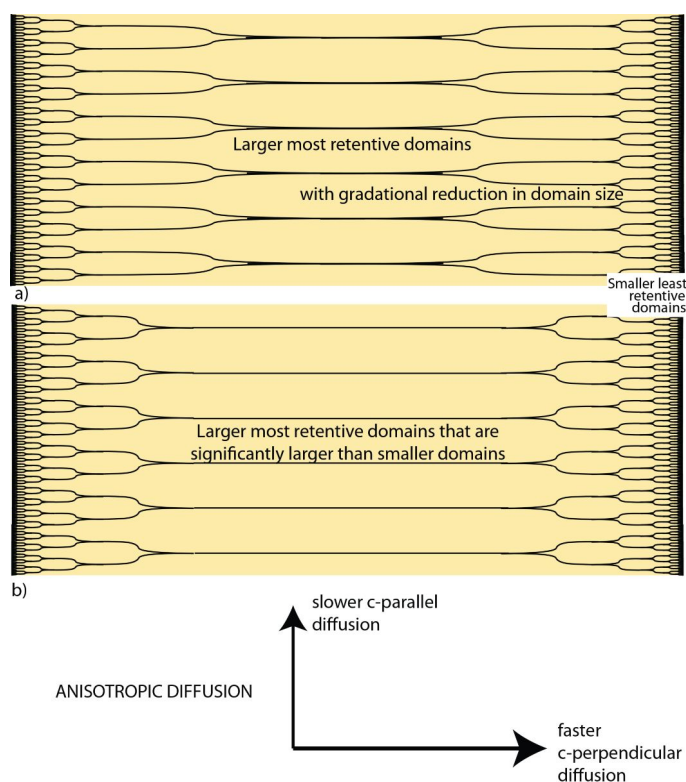
The source of the pebble cannot be known exactly. The most obvious source is from granites that are the closest to the Indus Formation, however the possibility that it may have been derived from a more distal source should also be considered. The Kohistan or Gangdese batholiths did have magmatic activity that was occurring in the early Paleogene during a second stage of plutonism (112-39 Ma), however the actual date of  $\sim 56$  Ma is not a common age (Heuberger *et al.* 2007, Wen *et al.* 2008, Treloar *et al.* 1989). In addition, the distances, and obstacles associated with transport of eroded pebbles to the Indus Formation make these batholiths an unlikely source. The Ladakh Batholith, immediately adjacent to the Indus Formation, is the most probable source as it preserves ages of 66-64 Ma, 60-56 Ma,  $\sim 49$ -45 Ma and 20-10 Ma (White *et al.* 2011, *cf.* Wu *et al.* 2007), and the petrology is equivalent. Our  $\sim 56$  Ma pebble is a granite by petrological classification (not a diorite or granodiorite), and we thus consider that it might represent an eroded equivalent of the  $56.5 \pm 1$  Ma Khardung La Granite, or the  $58 \pm 1$  Ma Chang La Granite from the Ladakh Batholith (White *et al.* 2011) as a source.

Importantly  $^{40}\text{Ar}/^{39}\text{Ar}$  geochronology on this pebble can be used to determine the relative timing of the regional events of both the Ladakh Batholith and the Indus Formation. For example, 16.5 Ma must be the maximum age of the formation of the molasse. In addition, 16.5 Ma must be the maximum age for the burial and deformation of the Indus Molasse, and the underlying Indus Formation. The sequence of tectonic events needed for this to happen is that the batholith must have been exhumed and eroded with deposits tumbled and abraded and then accreted to the Indus Formation prior to burial and deformation.

The diffusion parameters have been calculated applying the Fundamental Asymmetry Principle to the interpretation of Arrhenius data derived from the  $^{40}\text{Ar}/^{39}\text{Ar}$  step heating experiment. The following values have been obtained for a spherical geometry:  $E = 70.7$  kcal/mol and

$D0/r^2 = 4.90e+08s^{-1}$  rising to  $1.14e+06s^{-1}$  in the most retentive domains, where  $E$  is the activation energy and  $D0$  the frequency factor and  $r$  the domain radius. Fractal feathering (as described by Forster and Lister, 2010) can be seen to be a prominent feature in both the Arrhenius and the  $r/r_0$  plots. The activation energy would have been substantially underestimated if this FAP had not been observed.

Figure 14. Anisotropic diffusion modelling predicts faster c-perpendicular diffusion compared to the diffusion that would occur c-parallel



a) and b) show how different relative domain sizes of the fractal can emulate the  $r/r_0$  plot where:

1. assumes anisotropic diffusion, faster perpendicular to c-axis than parallel to it
2. assumes fractal pattern of very fast pathways (e.g. cleavage and/or stacking faults)
3. perhaps the Ca associated with the margins of such a fractal distribution allows the relative domain size of the fractal to emulate the  $r/r_0$  plot.

The diffusion parameters allow estimates as to the temperature during cooling, from which a depth can be inferred, based on assumptions on the temperature gradient. In essence, higher activation energies require higher temperatures to be maintained, and thus reflects the depth

at which preserved events have occurred. This in turn affects estimates as to exhumation rates and other aspects of tectonic interpretation. Note that the calculated activation energy for this sample is higher than that estimated from high-pressure experiments (Harrison *et al.* 2009). Modelling on anisotropic diffusion that predicts faster c-perpendicular diffusion compared to the diffusion that would occur c-parallel can be undertaken on this data (Figure 14). For example where different relative domain sizes of the fractal can emulate the  $r/r_0$  plot, different parameters can either assume anisotropic diffusion to be faster perpendicular to c-axis than parallel; or that the fractal pattern of very fast pathways exist (e.g. cleavage and/or stacking faults).

The Ladakh Batholith is reported to have a major pulse of magmatism active at ~56 Ma (White *et al.* 2011; Weinberg and Dunlap 2000; Upadhyay *et al.* 2008; Singh *et al.* 2007; Bhutani *et al.* 2009), and this is seen in the Chang La and Khardung La granites (White *et al.* 2011) which correlates well with the ~56 Ma age in the pebble. Metamorphic events recorded within the Ladakh Batholith have not been recorded in the Chang La or Khardung La granites, suggesting that localised activity, either structural or magmatic, has occurred. For example, the Chang La and Khardung La granites do not record evidence for the volcanic magmatism activity at ~47 Ma found elsewhere in the batholith (White *et al.* 2011; St-Onge *et al.* 2010; Weinberg and Dunlap 2000:  $^{40}\text{Ar}/^{39}\text{Ar}$  age of andesitic dyke); Bhutani *et al.* 2004:  $^{40}\text{Ar}/^{39}\text{Ar}$  age) and shear zone activity at for example 45 Ma in the Thanglagso Shear zone is localised to that zone (Weinberg and Dunlap 2000). However, Chang La granodiorites record the 20-10 Ma metamorphic event. No trace of a 49-45 Ma event was recorded from our pebble. This is again consistent with the suggestion that the Chang La or Khardung La granites are a possible source.

The Ladakh Batholith also preserves younger metamorphic or cooling ages (White *et al.* 2011: metamorphic zircon rims 10 - 20 Ma; Bhutani *et al.* 2003:  $^{40}\text{Ar}/^{39}\text{Ar}$  age; Kirstein 2011 and Kirstein *et al.* 2006: apatite+zircon fission track). These younger ages are consistent with the ages of the first steps of the  $^{40}\text{Ar}/^{39}\text{Ar}$  geochronology step-heating experiment undertaken in this study.

Other geochronometers have been used in this area to draw inferences as to the pattern of tectonic activity. Much of the tectonic interpretations from fission track ages are based on changing tilting directions of the

batholith (from north to south) over three distinct phases 49-30 Ma, 30-15 Ma and 15-0 Ma (Kirstein *et al.* 2009), where the Ladakh Batholith played a passive role in the regional tectonics during shortening associated with the India-Asia collision. This extensive fission track study (Kirstein 2011, Kirstein *et al.* 2006) suggests that magmatism ceased in the late Eocene with initial denudation driven by erosion due to uplift caused by large-scale shortening, with rapid exhumation and weathering between 35-26 Ma on the southern margin of the Ladakh Batholith. Apatite and zircon fission track and U-Th/He data from the central and northern edge of the Ladakh Batholith showed exhumation commenced after 18 Ma. The northern margin being exhumed at a rate of <0.4 mm/year from ~18 Ma (*cf.* Kirstein 2011), while exhumation in the central part of the batholith has been suggested to have been rapid and occurred at ~22 Ma (Kirstein 2011). What can be said is that younger ages are being recorded in association with exhumation of this batholith whether they be SHRIMP ages,  $^{40}\text{Ar}/^{39}\text{Ar}$  geochronology ages or fission track ages.

Shear zones within, and on the carapace of the Ladakh Batholith suggest that it was not a massive passive block that tilted with regional tectonics but was rather deformed, or was ductilely ripped apart by movement on regional-scale shear zones during its history. The structural features that we observed on the southern margin of the Ladakh Batholith (Fig. 1c) were occasional bounding southwest dipping ductile shear zones. These structures appear to define remnants of a carapace shear zone, as occurs with a metamorphic core complex. For the Indus Molasse to be made from pebbles of the Ladakh Batholith itself, it first must have been exhumed, allowing the batholith to be eroded and debris transported. These pebbles (and cobbles etc.) then accumulated and accreted onto the Indus Formation. According to this hypothesis, parts of the Indus Formation are a molasse that formed as an apron at the margins of the Ladakh core complex, after its Miocene exhumation, once the lower plate was exposed. We suggest that the movement of the late back thrusting of the Indus Formation with the Indus Molasse is thus Miocene or younger.

Microstructural analysis of a pebble within the Indus Molasse in conjunction with  $^{40}\text{Ar}/^{39}\text{Ar}$  age results from this study indicate that the pebble was eroded from the source, suggested here as the Ladakh Batholith, some time after 16.5 Ma, during its continued extensional

exhumation. This produced a molasse that accreted to the Indus Formation. The upright folding observed in the Indus Formation (and Indus Molasse) during inversion of the core complex took place at a later time, i.e. mid-Miocene or younger. The sequence of events that allows a pebble from the Ladakh Batholith to be consolidated and deformed into the overlying material is possible when it is considered that the later inversion of the region resulted in back-thrusting, and recumbent folds (Fig. 1b). These in turn were overprinted by later tight upright folds, during which time a pervasive axial plane slaty cleavage was formed, overprinting earlier formed structures (Fig. 1b).

The way in which the Indus Formation is backthrust over the Indus molasse is similar to tectonic sequences that occurred in Tibet where the Xigaze terrane is thrust back over the Gangrinboche conglomerates (Gansser 1964; Aitchison *et al.* 2007). In addition, earlier studies on the Tibet uplift or unroofing of correlative rocks (Transhimalayan batholith also known as the Gangdese batholith) suggest that southern Tibet was significantly uplifted and eroded in the early Miocene (Harrison *et al.* 1992), at about the same time as our data suggests for the Ladakh Batholith and formation of the Indus Molasse in Indus Suture region.

## Conclusion

We suggest that the Indus Formation is overlain by a molasse that formed as an apron at the margins of the Ladakh Batholith, as it was exhumed by extensional shear zones, as would occur during exposure of a core complex. Material eroded from the batholith was transported and accumulated onto the topographically lower, but structurally higher Indus Formation (in the upper plate of the south-dipping extensional faults formed at the margin of the batholith). Later inversion resulted in back thrusting of the Indus Formation and overlying Indus Molasse, towards the north, back over the Ladakh Batholith. This back-thrusting led to the formation of recumbent folds overprinted by tight upright folds.

From this data emerges the view that, at one stage within a relatively complex history of accretion during convergence of India and Asia, the exhumation of a sequence of metamorphic core complexes took place as the result of a period of widespread extensional tectonism from mid-Miocene or younger. Finally, Himalayan orogenesis resulted in renewed crustal shortening, and

inverted the southern margin of the Ladakh core complex, deforming the Indus Formation and the Indus Molasse as a single unit.

### Acknowledgments

M.A. Forster acknowledges the support of an Australian Research Fellowship provided by the Australian Research Council (ARC) associated with the Discovery grants DP0877274, and additional support from the Research School of Earth Sciences at The Australian National University (ANU).  $^{40}\text{Ar}/^{39}\text{Ar}$  analysis was done in

the Argon Geochronology Facility at ANU. Irradiation of the sample was done at McMaster Reactor, Canada. The *eArgon* software used in the paper was written by G.S. Lister. G.S. Lister is gratefully acknowledged for fieldwork initiation and involvement as well as vital discussion. Discussion with J. Aitchison greatly appreciated. T. Ireland gave support for SHRIMP analysis at ANU. Jia-Urn Lee undertook SEM white mica analysis at EMU, ANU. Support in Ladakh from Dr. C.P. Dorjey is gratefully acknowledged. The paper is much improved by the two reviewers A. Camacho and J. Aitchison.

## References

- Aitchison, J.C., Davis, A.M., Badengzhu, Luo, H. 2002. New constrains on the India-Asia collision: the lower Miocene Gangrinboche conglomerates, Yarlung Tspangpo suture zone, SE Tibet. *Journal of Asian Earth Sciences*, 21, 251-263.
- Aitchison, J.C., Ali, J.R. and David, A.M. 2007. When and where did India and Asia collide? *Journal of Geophysical Research*, 112, B05423, 10.1029/2006JB004706, 2007
- Aitchison, J. C., Xia, X., Baxter, A. T., Ali, J. R. 2011. Detrital zircon U-Pb ages along the Yarlung-Tsangpo suture zone, Tibet: Implications for oblique convergence and collision between India and Asia. *Gondwana Research*, 20, 691-709.
- Auden, J.B., 1933. On the age of certain Himalayan granites. *Records Geological Survey India, Calcutta*, 66: 461-471.
- Bhutani R., Pande K. and Desai, N. 2003. Age of the Karakoram fault activation: 40Ar-39Ar geochronological study of Shyok suture zone in northern Ladakh, India. *Current Science*, 84, 1454-158
- Bhutani R., Pande K., Venkatesan, T.R. 2004. Tectono-thermal evolution of the India-Asia collision zone based on 40Ar-39Ar thermochronology in Ladakh, India. *Proc. Indian Acad. Sci. (Earth Planet. Sci)*, 113, 737-754.
- Bhutani R., Pande K., Venkatesan, T.R. 2009. 40Ar-39Ar dating of volcanic rocks of the Shyok suture zone in north-west trans-Himalaya: Implications for the post-collision evolution of the Shyok suture zone. *Journal of Asian Earth Sciences* 34, 168-177.
- Bröcker, M., Kreuzer, H., Matthews, A., and Okrusch, M. 1993 40Ar/39Ar and oxygen isotope studies of polymetamorphism from Tinos Island, Cycladic blueschist belt, Greece. *Journal metamorphic Geology*, 11, 223-240.
- Clift, P.D., Shimizu, N., Layne, G.D., Blusztajn, J. 2001. Tracing patterns of erosion and drainage in the Paleogene Himalaya through ion probe Pb isotope analysis of detrital K-feldspars in the Indus Molasse, India. *Earth and Planetary Science Letters* 188, Issues 3-4, 15, 475-491. 10.1016/S0012-821X(01)00346-6
- Clift, P.D., Carter, A., Krol, M., Kirby, E., 2002. Constraints on India-Eurasia collision in the Arabian Sea region taken from the Indus Group, Ladakh Himalaya, India. In: Clift, P.D., Kroon, D., Gaedicke, C., Craig, J. (Eds.), *The Tectonic and Climatic Evolution of the Arabian Sea Region*. Geological Society Special Publications, London, pp. 97-116.
- Davis, A. M., Aitchison, J. C., Badengzhu, and Hui, L. 2004. Conglomerates record the tectonic evolution of the Yarlung-Tsangpo suture zone in southern Tibet. *Geological Society, London, Special Publications*, 226, 235-246.
- Forster and Lister 2010. Argon enters the retentive zone: reassessment of diffusion parameters for K-feldspar in the South Cyclades Shear Zone, Ios, Greece. *Geological Society, London, Special Publications*. 332; p. 17-34. 10.1144/SP332.2
- Gansser, A., *Geology of the Himalayas*, 289 pp., Wiley-Interscience, New York, 1964.
- Gansser, A. 1980. The significance of the Himalayan Suture Zone, *Tectonophysics*, 62, 37-52.
- Garzanti, E., and Van Haver, T. 1988. The Indus clastics: forearc basin sedimentation in the Ladakh Himalaya (India): *Sedimentary Geology*, 59, 237-249.
- Guillot, S., Mahéo, G., de Sigoyer, J., Hattori, K.H., Pecher, A. 2008. Tethyan and Indian subduction viewed from the Himalayan high- to ultrahigh-pressure metamorphic rocks. *Tectonophysics* 451, 225-241.
- Heuberger, S., Sschallegger, U., Burg, J-P., Villa, I.M., Frank, M., Dawood, H., Hussain, S. and Zanchi, A. 2007. Age and isotopic constraints on magmatism along the Karakoram-Kohistan Suture Zone, NW Pakistan: evidence for subduction and continued convergence after India-Asia collision. *Swiss j. geosci.* 100 (2007) 85-107. DOI 10.1007/s00015-007-1203-7
- Harrison, T.M., Copeland, P., Kidd, W.S.F. and Yin, A. 1992. Raising Tibet. *Science*, 255, 1663-1670.
- Harrison, T.M., Copeland, P., Hall, S.A., Quade, J., Burner, S., Ojha, T. P. and Kidd, W. S. F. 1993. Isotopic Preservation of Himalayan/Tibetan Uplift, Denudation, and Climatic Histories of Two Molasse Deposits'. *The Journal of Geology*, Vol. 101, No. 2, 100th Anniversary Symposium: Evolution of the Earth's Surface (Mar., 1993), pp. 157-175.
- Harrison, T.M., Célérier, J., Aikman, A.B., Hermann, J., Heizler, M.T. 2009. Diffusion of 40Ar in muscovite. *Geochimica et Cosmochimica Acta*, 73, 1039-1051.
- Kirstein, L.A. 2011. Thermal evolution and exhumation of the Ladakh Batholith, northwest Himalaya, India. *Tectonophysics* 503 222-233. 10.1016/j.tecto.2011.03.005
- Kirstein, L.A., Foeken, J.P.T., Van der Beek, P., Stuart, F.M., and Phillips, R.J. 2009. Cenozoic unroofing history of the Ladakh Batholith, western Himalaya, constrained by thermochronology and numerical modeling: *Journal of the Geological Society of London*, 166, 667-678. 10.1016/j.gca.2003.10.021.
- Kirstein, L.A., Sinclair, H., Stuart, F.M., Dobson, K., 2006. Rapid Early Miocene exhumation of the Ladakh Batholith, northwestern Himalaya. *Geology* 34, 1049-1052.
- Lovera, O.M., Grove, M, Harrison, T.M. and Mahon, K.I. 1997. Systematic analysis of K-feldspar 40Ar/39Ar step heating results: I. significance of activation energy determinations. *Geochimica et Cosmochimica Acta* 61, 3171-3192.
- McDougall, I. and Harrison, T.M. 1999. *Geochronology and Thermochronology by the 40Ar/39Ar Method*. 2nd edition, 269pp., Oxford Univ. Press, New York.

- Najman, Y., Johnson, K., White, N., and Oliver, G. 2004. Evolution of the Himalayan foreland basin, NW India, *Basin Research*, 16, 1-24.
- Rowley, D.B. 1996. Age of initiation of collision between India and Asia: A review of stratigraphic data: *Earth and Planetary Science Letters*, 145, 1-13.
- Singh, S., Kumar, R., Barley, M.E., Jain, A.K., 2007. SHRIMP U-Pb ages and depth of emplacement of Ladakh Batholith, Eastern Ladakh, India. *Journal of Asian Earth Sciences* 30 (3-4), 490-503.
- Searle, M.P., Pickering, K.T. and Cooper, D.J.W. 1990. Restoration and evolution of the intermontane Indus molasse basin, Ladakh Himalaya, India. *Tectonophysics*, 174, 301-314.
- Schlup, M., Carter, A., Cosca, M., Steck, A. 2003. Exhumation history of eastern Ladakh revealed by  $^{40}\text{Ar}$ - $^{39}\text{Ar}$  and fission track ages: the Indus River-Tso Moriri transect, NW Himalaya. *Journal of the Geological Society of London* 160, 385-399.
- Sinclair, H.D. and Jaffey, N. 2001. Sedimentation of the Indus Group, Ladakh, northern India: implications for the timing of initiation of the palaeo-Indus River: *Journal of the Geological Society, London*, 158, 151-162.
- Spell, T and McDougall, I. 2003. Characterization and calibration of  $^{40}\text{Ar}/^{39}\text{Ar}$  dating standards. *Chemical Geology* 198 (2003) 189- 211.
- Steiger, R. H., and E. Jager (1977), Subcommittee on geochronology: Convention on the use of decay constants in geo- and cosmochronology, *Earth Planet. Sci. Lett.*, 36, 359-362.
- Stern, L.A., Chamberlain, C.P., Reynolds, R.C. and Johnson, G.D. 1997. Oxygen isotope evidence of climate change from pedogenic clay minerals in the Himalayan molasse *Geochimica et Cosmochimica Acta*, 61, 731-744. 10.1016/S0016-7037(96)00367-5
- St-Onge, M.R., Rayner, N., Searle, M.P., 2010. Zircon age determinations for the Ladakh batholith at Chumathang (Northwest India): implications for the age of the India-Asia collision in the Ladakh Himalaya. *Tectonophysics* 495, 171-183.
- Thakur, V. C., and Misra, D. K. 1984. Tectonic framework of the Indus and Shyok suture zones in eastern Ladakh, northwest Himalaya, *Tectonophysics*, 101, 207-220.
- Treloar, P.J., Rex, D.C., Guise, P.G., Coward, M.P., Searle, M.P., Windley, B.F., Petterson, M.G., Jan, M.Q., Luff, I.W., 1989. K/Ar and Ar/Ar geochronology of the Himalayan collision in NW Pakistan: constraints on the timing of suturing, deformation, metamorphism and uplift. *Tectonics* 8, 881-909.
- Upadhyay, R., Frisch, W. and Siebel, W. 2008. Tectonic implications of new U-Pb zircon ages of the Ladakh batholith, Indus suture zone, northwest Himalaya, India. *Terra Nova*, 20, 309-317. 10.1111/j.1365-3121.2008.00822.x
- Weinberg, R.F., Dunlap, W.J., 2000. Growth and deformation of the Ladakh batholith, Northwest Himalayas: implications for timing of continental collision and origin of calc-alkaline batholith. *J. Geol.* 108, 303-320.
- Wen, D.-R., et al., 2008. Zircon SHRIMP U-Pb ages of the Gangdese Batholith and implications for Neotethyan subduction in southern Tibet. *Chemical Geology* 252 (3-4), 191-201.
- White, L. T., Ahmad, T., Ireland, T.R., Lister, G.S., Forster, M.A. 2011. Deconvolving episodic age spectra from zircons of the Ladakh Batholith, northwest Indian Himalaya, *Chemical Geology* [10.1016/j.chemgeo.2011.07.024].
- Wu, F., Clift, P.D., and Yang, J., 2007. Zircon Hf isotopic constraints on the sources of the Indus Molasse, Ladakh Himalaya, India: *Tectonics*, p. 10.1029/2006TC002051

## A. Appendix A.

 Table 1.  $^{40}\text{Ar}/^{39}\text{Ar}$  table for LAD06-01 Pebble

Temp (°C)	Ar36 (mol)	Ar37 (mol)	Ar39 (mol)	Ar40 (mol)	% Ar40*	Ar40* / Ar39 K	Cumulative Ar39 (%)	Calculated age (Ma)	1 $\sigma$	Ca/K
450	1.40E-16	2.91E-17	3.72E-16	4.42E-14	6.1	7.27	0.05	22.69	$\pm 10.3$ 5	1.49E-01
500	1.40E-16	5.68E-17	6.34E-16	4.46E-14	7.5	5.28	0.15	16.5	$\pm 4.75$	1.70E-01
550	1.14E-16	4.89E-17	1.10E-15	4.23E-14	20.1	7.69	0.30	24.01	$\pm 2.49$	8.43E-02
600	1.29E-16	9.84E-17	2.13E-15	5.66E-14	32.6	8.66	0.61	27.02	$\pm 0.74$	8.77E-02
650	1.05E-16	3.20E-16	4.26E-15	7.74E-14	59.8	10.85	1.23	33.79	$\pm 0.79$	1.43E-01
650	8.86E-17	9.06E-16	9.06E-15	1.36E-13	80.6	12.11	2.53	37.67	$\pm 0.15$	1.90E-01
740	5.89E-17	1.17E-15	1.23E-14	1.84E-13	90.4	13.52	4.31	41.98	$\pm 0.17$	1.81E-01
770	6.06E-17	3.27E-15	1.41E-14	2.21E-13	91.9	14.44	6.33	44.81	$\pm 0.15$	4.42E-01
800	5.84E-17	4.56E-15	1.76E-14	2.88E-13	94.0	15.38	8.88	47.7	$\pm 0.18$	4.91E-01
830	6.30E-17	1.08E-14	2.27E-14	3.87E-13	95.3	16.23	12.15	50.29	$\pm 0.06$	9.04E-01
850	5.38E-17	7.97E-15	2.45E-14	4.26E-13	96.3	16.76	15.69	51.91	$\pm 0.12$	6.18E-01
870	5.51E-17	6.58E-15	3.18E-14	5.64E-13	97.1	17.22	20.27	53.3	$\pm 0.09$	3.93E-01
890	6.44E-17	2.28E-15	4.40E-14	7.97E-13	97.5	17.67	26.62	54.69	$\pm 0.09$	9.83E-02
910	5.71E-17	1.83E-15	5.47E-14	1.01E-12	98.2	18.08	34.51	55.94	$\pm 0.14$	6.35E-02
930	5.72E-17	1.41E-15	5.07E-14	9.28E-13	98.0	17.95	41.82	55.56	$\pm 0.11$	5.27E-02
950	6.12E-17	1.49E-15	5.49E-14	1.00E-12	98.1	17.85	49.74	55.24	$\pm 0.19$	5.17E-02
970	6.27E-17	2.94E-15	5.26E-14	9.70E-13	98.0	18.08	57.32	55.94	$\pm 0.32$	1.06E-01
990	6.88E-17	3.89E-15	5.41E-14	1.00E-12	97.9	18.08	65.13	55.93	$\pm 0.37$	1.37E-01
1020	8.68E-17	2.81E-15	7.70E-14	1.45E-12	98.1	18.44	76.24	57.03	$\pm 0.16$	6.93E-02
1050	8.06E-17	1.35E-15	7.34E-14	1.40E-12	98.2	18.75	86.83	57.98	$\pm 0.13$	3.50E-02
1080	6.71E-17	2.31E-15	6.19E-14	1.22E-12	98.3	19.34	95.76	59.79	$\pm 0.17$	7.09E-02
1110	8.15E-17	4.66E-15	2.43E-14	5.05E-13	95.2	19.78	99.27	61.11	$\pm 0.26$	3.64E-01
1160	1.19E-16	9.94E-15	2.80E-15	8.78E-14	60.9	19.14	99.67	59.16	$\pm 1.34$	6.77E+00
1220	1.78E-16	9.28E-15	1.23E-15	7.96E-14	35.1	22.91	99.85	70.58	$\pm 1.94$	1.45E+01
1350	4.05E-16	4.25E-15	5.75E-16	1.33E-13	10.3	23.91	99.93	73.61	$\pm 11.2$	1.41E+01
1450	9.63E-16	1.67E-15	4.85E-16	2.93E-13	3.0	18.02	100.00	55.76	$\pm 38.4$	6.57E+00
<b>Total</b>	3.42E-15	8.59E-14	6.93E-13	1.33E-11		17.77		55	$\pm 0.24$	

## Notes for table 1

Table colour coding correlates to the colour coding in the analysis of data plots. Flux monitor ages are taken from Spell and McDougall (2003).  $^{40}\text{K}$  abundances and decay constants are taken from standard values recommended by the IUGS subcommission on Geochronology (Steiger and

Jager, 1977).  $\text{Lambda } K^{40} = 5.5430\text{E-}10$   
 $J=0.0017419 \pm 0.47$ ; Flux Monitor: sanidine 92-176, at  $28.10 \pm 0.04$  Ma (Spell and McDougall 2003); Irradiated for 18 MWh in position 5C at McMasters Reactor. Correction Factors:  $^{36}\text{Ar}/^{37}\text{Ar}$   $3.50\text{E-}4$ ;  $^{39}\text{Ar}/^{37}\text{Ar}$   $7.86\text{E-}4$ ;  $^{40}\text{Ar}/^{39}\text{Ar}$   $2.7\text{E-}2$